ACS APPLIED NANO MATERIALS
Cite This: ACS Appl. Nano Mater. 2019, 2, 440−451
Article
www.acsanm.org

Enhanced Thermal Conductivity in Polymer Nanocomposites via Covalent Functionalization of Boron Nitride Nanotubes with Short Polyethylene Chains for Heat-Transfer Applications

Susana Quiles-Díaz,[†] Yadienka Martínez-Rubí,[‡] Jingwen Guan,[‡] Keun Su Kim,[‡] Martin Couillard,[§] Horacio J. Salavagione,*[,†] Marián A. Gómez-Fatou,[†] and Benoit Simard[‡]

[†]Departamento de Física de Polímeros, Elastómeros y Aplicaciones Energéticas, Instituto de Ciencia y Tecnología de Polímeros (ICTP-CSIC), Juan de la Cierva 3, 28006 Madrid, Spain

[‡]Security and Disruptive Technologies Research Centre, Emerging Technologies Division, National Research Council Canada, Ottawa, Ontario K1A 0R6, Canada

[§]Energy, Mining and Environment Research Centre, Engineering Division, Emerging Technologies Division, National Research Council Canada, Ottawa, Ontario K1A 0R6, Canada

Supporting Information

ABSTRACT: Boron nitride, which possesses high thermal conductivity, is often incorporated into polymer matrixes for thermal management. The enhancement in the thermal conductivity depends on the filler shape, size, effective dispersion in the matrix, and interfacial thermal resistance between the filler and matrix, and the last two are the most challenging issues. To address these challenges, in this study two different covalent functionalization approaches on boron nitride nanotubes (BNNTs) with short polyethylene (PE) chains are employed: one based on the Williamson reaction and the other on nitrene [1 + 2] chemistry. The covalent connection between the nanotubes and the polymer is confirmed by Fourier transform infrared, X-ray photoelectron microscopy, tandem thermogravimetric−infrared spectroscopy analysis and energy-filtered transmission electron microscopy. The modification of BNNTs with short polymer chains has resulted in an excellent strategy to modulate the interface in polymer composites. Tuning the interface has a strong influence on thermal transport, and up to an ∼250% increase in the thermal conductivity of BNNT-HDPE nanocomposites has been observed when the loading increases from 20 to 40 wt % of PE-modified BNNTs due to the improved dispersion and reduced interfacial thermal resistance. The materials described here show the potential for heat-transfer applications.

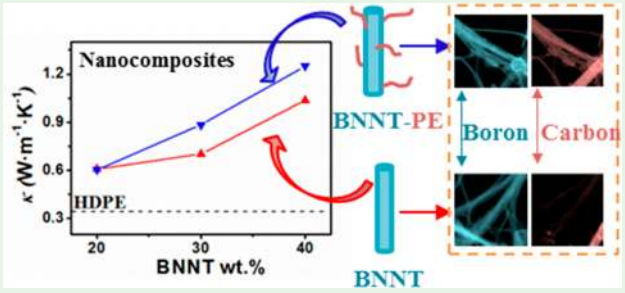

KEYWORDS: *thermal management, flexible heat conductors, polymer brushes, Williamson reaction, nitrene chemistry*

INTRODUCTION

Nowadays, materials for heat-transfer applications require light weight, flexibility, a stable mechanical performance, easy processing and low cost. Polymers accomplish these characteristics even though they have lower thermal conductivity compared to commonly employed materials.

Polymer nanocomposites containing boron nitride have been widely investigated for thermal management because they are light-weight materials with extreme ratios of thermal-to-electrical conductivity because of the electrical insulating nature of boron nitride (BN).[1−4] As is widely known, achieving superior properties, like thermal conductivity for instance, strongly depends on the filler/polymer interface, which is governed by several factors, as was recently highlighted.[5] Chemical modification of fillers in order to enhance the polymer/filler interface contact is envisaged as a very powerful tool.[1] However, although some advances in the chemical functionalization of boron nitride (e.g., h-BN) have been reported,[6−10] the chemistry of such a material is limited. By analogy with the chemical reactivities of graphene and carbon nanotubes (CNTs), where the latter are more reactive because of bond tensions resulting from the curved structure, the same behavior can be expected for 2D sheets and nanotubes of BN.

Boron nitride nanotubes (BNNTs) have emerged as promising nanomaterials for the development of new technologies and multifunctional materials for engineering applications and drawn interest among the scientific community because of their outstanding properties, such as high mechanical stiffness, wide band gap, chemical stability, excellent thermal conductivity and thermal stability.[11] Never-

Received: November 5, 2018
Accepted: December 20, 2018
Published: December 20, 2018

DOI: 10.1021/acsanm.8b01992
ACS Appl. Nano Mater. 2019, 2, 440−451

theless, their application has been hindered by the lack of a production method able to produce sufficient quantities of material. Recent advances in the large-scale production of high-quality and high-purity BNNTs by laser and thermal plasma processes[12−14] have promoted an advancing research on BNNT applications.

BNNTs have gained great attention as functional fillers to reinforce polymer matrixes, with the aim of producing high-performance polymer nanocomposites.[15−22] However, the development of polymer nanocomposites reinforced with BNNTs is not straightforward, and several drawbacks must be addressed. The principal disadvantage is the natural tendency of BNNTs, like other nanomaterials, to agglomerate in bundles because of van der Waals interactions. Because of their high aspect ratios, these interactions are very strong and persist when the BNNTs are incorporated into polymer matrixes, yielding poor dispersion. Moreover, a strong BNNT/polymer interface must be achieved to ensure the optimal transfer of properties from the filler to the matrix. In the case of CNTs, the dispersion and interface strength can be improved by many proven surface modification strategies;[23,24] however, the case of BNNTs is more challenging because the chemistry of BNNTs is poorly developed. Although BNNTs are structurally similar to CNTs, their chemistries are vastly different because of the differences in bonding character brought about by the different electronic structures.[25,26] Consequently, the advancement of BNNT surface modification methods is required in order to produce BNNT-based materials with superior properties.

Currently, there are few reports for the direct functionalization of pristine BNNTs.[27,28] Shin et al.[27] proposed a promising route based on the chemical reduction of the nanotube, using sodium naphthalide, followed by reactions with free radicals. They succeeded in covalently functionalizing BNNTs with hexyl chains. Moreover, Lin et al.[28] covalently functionalized BNNTs using thermally labile peroxides that can decompose to generate radicals that are able to react with the nanotubes via a Lewis acid−base reaction. However, the most common approach consists of a two-step method of "activation" with functional surface groups (−OH or $-NH_2$), followed by reaction with target molecules.[29−32] One of the pioneering works involving two reaction steps was reported by Ciofani et al.,[29] who introduced hydroxyl groups onto the BNNT surface by means of a strong oxidation process that was followed by silanization of the surface with (3-aminopropyl)triethoylsilane. A third approach takes advantage of the amino groups present at the surface of the BNNTs produced under specific conditions.[30,33] It should be highlighted that significantly more effort has been devoted to the direct functionalization of hexagonal boron nitride nanosheets (BNNSs).[34−36] In this regard, Sainsbury et al.[36] presented a covalent functionalization approach of BNNSs by using the reactivity of the nitrene radicals produced by the thermolysis of (4-methoxybenzyl)-oxycarbonyl azide, where the labile nitrene is able to react with the electron-deficient boron atom.

All of the above-mentioned strategies deal with the covalent incorporation of discrete organic molecules. However, a very attractive approach to enhancing the BNNT/polymer interface in nanocomposites consists on the functionalization of BNNTs with low-molecular-weight polymers. These polymer-modified BNNTs can be used as fillers for higher-molecular-weight polymers, with the aim of developing high density of supramolecular interactions between both components. This enhanced filler/matrix affinity is expected to significantly increase the strength and quality of the interface, as demonstrated for the nanocomposites with polymer-functionalized graphitic nanofillers,[37−41] and to reduce the interfacial thermal resistance because the energy of the phonon modes of the side chains is closer to those of the target matrix.

Up to now, investigations of the chemical functionalization of BN nanomaterials with polymers were limited to a few examples and mainly related with BNNSs instead of BNNTs.[42−45] In addition, the BN nanomaterial was acting, in most cases, as a polymerization platform for the growth of polymer chains (grafting-from).[43−45] This strategy ensures that both the grafting of relatively high-molecular-weight polymers and high grafting ratios are achieved but with the drawback of requiring complex synthetic routes to incorporate the polymerization initiator onto the BN surface.[46,47]

In this paper, we report the functionalization of BNNTs with short PE brushes (∼460 $g{\cdot}mol^{-1}$) following a grafting-to approach. In our particular case, grafting-to provides a number of advantages because the reaction is addressed in a single step and a low degree of functionalization is obtained, which is positive in terms of minimizing BNNT framework damage. Here, two synthetic strategies are reported. The first one was inspired by the Williamson reaction[48] for the synthesis of ethers, where hydroxylated BNNT (BNNT-OH) is reacted with a bromine-terminated polyethylene (PE-Br); the second strategy consists of the reaction between pristine BNNTs and azide-terminated polyethylene (PE-N_3). Further, BNNT-N-PE is selected and integrated into a high-density polyethylene matrix for evaluation.

EXPERIMENTAL SECTION

Materials. High-density polyethylene (HDPE; Alcudia HDPE 47100) from Repsol has M_w (157870 $g{\cdot}mol^{-1}$) and polydispersity index (11) experimentally determined by gel permeation chromatography in 1,2,4-trichlorobenzene.

Raw BNNTs were synthesized by the hydrogen-assisted BNNT synthesis method.[12] These BNNTs have few walls (2−5 walls) and an average diameter of 5 nm. A hexagonal boron nitride (BN) powder (99.5%, 70 nm, MK-hBN-N70, M K Impex Corp.) was used as the feedstock. Raw BNNTs contained about 25 wt % of boron particles and 25 wt % of nontubular BN species; hence, prior to being used for chemical functionalization with PE, they were purified through a combination of thermal and solvent treatments. The raw BNNTs have been purified using two approaches. In one approach, chlorine-phase thermal treatment at 750 °C followed by solvent extraction was used to remove elemental boron and some h-BN.[49] This material is labeled BNNT in the paper. Thermogravimetric analysis (TGA) and scanning electron microscopy (SEM) indicate a purity of about 70 wt %, with the rest being BN impurities. In the second approach, a low-purity BNNT material was treated with excess liquid bromine in water for surface hydroxyl functionalization. This material is labeled BNNT-OH[50,51] and has a purity, estimated by SEM, of ∼50 wt %. SEM was used to determine the collective/representative purity level of BNNTs through the entire sample area (not determined on a single image) by estimating the relative ratio of the appearances of nontubularstructures (named impurities collectively) and tubularstructures (named pure BNNT tubes).

As previously mentioned, two different approaches were developed to functionalize the BNNTs with PE chains. Each strategy requires the use of a different PE reactant, bromide or azide-terminated PE (PE-Br or PE-N_3). Both precursors are converted from PE monoalcohol (PE-OH; M_n = 460 $g{\cdot}mol^{-1}$, Aldrich), following a reported procedure.[38] Triacontane (Aldrich), a linear alkane with 30 carbon atoms, M_w= 422 $g{\cdot}mol^{-1}$ resembling the short polymer chains that have reacted with BNNT, was used to carry out control reactions. All solvents,

DOI: 10.1021/acsanm.8b01992
ACS Appl. Nano Mater. 2019, 2, 440−451

Scheme 1. Illustration of the Different Approaches Designed To Covalently Functionalize BNNT Surfaces with Short PE Chains

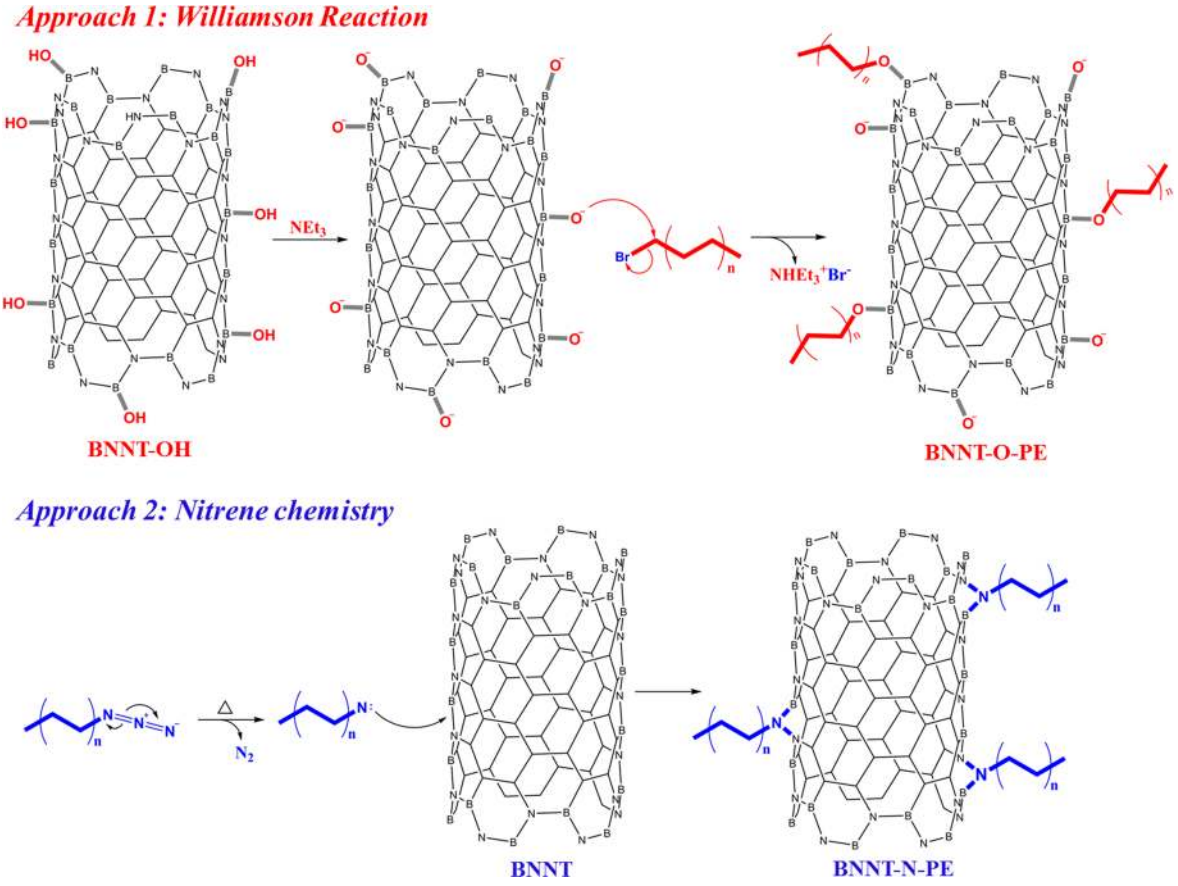

triethylamine (NEt_3; Aldrich), dimethylformamide (DMF; Aldrich), and anhydrous toluene (Aldrich), were used as received.

Preparation of PE-Grafted BNNTs. The approaches used to functionalize BNNTs with PE chains are illustrated in Scheme 1.

Approach 1. Williamson Reaction, BNNT-O-PE. The covalent functionalization of BNNT-OH via the Williamson reaction took place in two steps under a dry atmosphere. First, BNNT-OH was deprotonated by using NEt_3. Second, the reactive deprotonated BNNT-O^- reacted with the bromine-terminated PE via a S_N2 reaction. The reaction was carried out as follows: 50 mg of BNNT-OH (1.94 mmol) was dispersed in 150 mL of anhydrous toluene by bath sonication for 15 min, and then 7 mL of NEt_3 (50 mmol) was added to the BNNT-OH suspension. The reaction mixture was stirred at 110 °C for 3 h to achieve the appropriate deprotonation level. Afterward, 500 mg of PE-Br (0.96 mmol) was completely dissolved in 50 mL of anhydrous toluene at 65 °C and then added to the nanotube dispersion. The resulting mixture was refluxed for 42 h. Afterward, the mixture was cooled to 65 °C and the reaction product, BNNT-O-PE, was collected by vacuum filtration using a poly(tetrafluoroethylene) (PTFE) membrane filter with a pore size of 0.2 μm. The crude product was extracted twice with 200 mL of toluene at 110 °C for 2 h each time to remove any nonreacted polymer. The reaction product was filtered after each toluene wash, and, finally, a single wash of the product with 90 mL of DMF for 90 min was carried out to remove the $NEt_3^+Br^-$ salt generated as the byproduct. Last, the product was washed once again with 200 mL of hot toluene and dried at 100 °C for 12 h.

A control reaction was also performed. It consisted of dispersing 50 mg of BNNT-OH in 150 mL of toluene with the aid of bath sonication for 15 min. Then, 400 mg of triacontane (0.95 mmol) was completely dissolved in 50 mL of toluene at 65 °C and added to the nanotube dispersion. The resulting mixture was heated at 70 °C for 24 h under stirring. Furthermore, the control reaction product was also exhaustively purified following the same protocol as that described above and denoted as the Williamson control.

Approach 2. Nitrene Chemistry, BNNT-N-PE. The functionalization of BNNTs via nitrene [1 + 2] addition was achieved by thermolysis of the azide-terminated PE in the presence of BNNT under a nitrogen atmosphere. First, 80 mg of BNNTs (3.22 mmol) was dispersed in 200 mL of DMF and bath-sonicated for 15 min. Then, 500 mg of PE-N_3 (1.03 mmol) was added to the BNNT suspension. The resulting mixture was stirred and refluxed for 48 h. The large excess of PE-N_3 was used to ensure that the nanotubes were exposed to the maximum number of reactive species possible. Then, the mixture was cooled to 70 °C, and the reaction product, BNNT-N-PE, was collected by vacuum filtration. The reaction product was also exhaustively washed to ensure the removal of any nonreacted polymer. The purification procedure consisted of three consecutive washes with 200 mL of hot toluene (110 °C), with each wash lasting for 2 h. After each wash, the reaction product was collected by vacuum filtration on a PTFE membrane with a pore size of 1.2 μm. Then, in order to remove residual DMF that might be present with the nanotubes, the sample was stirred overnight with 200 mL of deionized water at room temperature. The product was collected by vacuum filtration, and the nanotubes were further rinsed with 200 mL of methanol. Last, the sample was dried at room temperature for 96 h.

As in route 1, a control reaction was again performed. For that, 50 mg of BNNT (2.01 mmol) was dispersed in 125 mL of DMF with the aid of bath sonication for 15 min. Then, 312 mg of triacontane (0.74 mmol) was completely dissolved in 30 mL of toluene at 65 °C and added to the nanotube dispersion. The resulting mixture was heated at 65 °C for 24 h under stirring. Then, the product was exhaustively purified following the same protocol as that described above. This sample is named as the azide control.

Preparation of BNNT/HDPE Nanocomposites. BNNT-N-PE prepared by approach 2 was selected as the filler for HDPE and

DOI: 10.1021/acsanm.8b01992
ACS Appl. Nano Mater. 2019, 2, 440−451

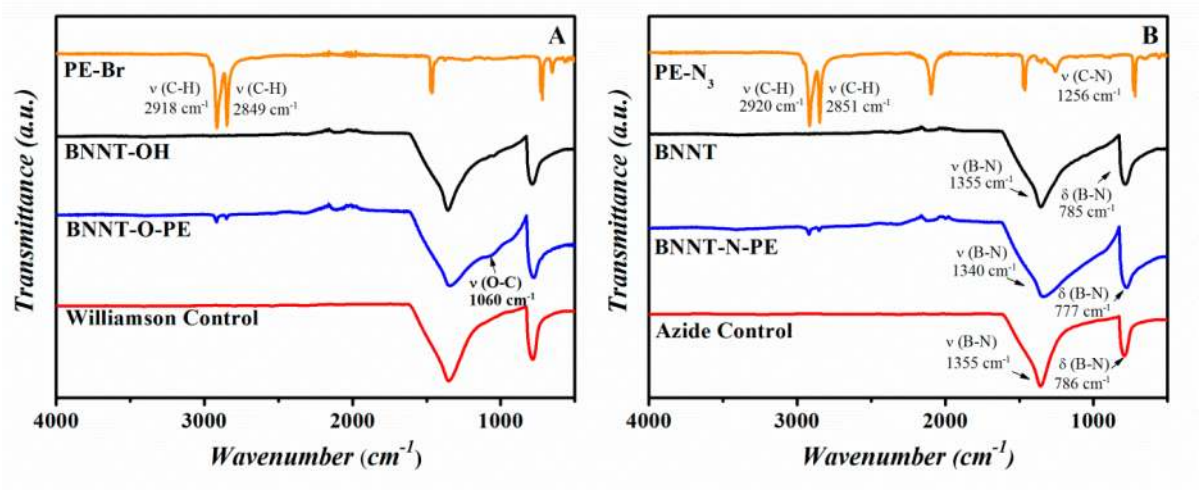

Figure 1. FTIR spectra of PE-Br, BNNT-OH, BNNT-O-PE, and the Williamson control reaction product (A) and PE-N_3, BNNT, BNNT-N-PE, and the azide control reaction product (B).

denoted as mBNNT. Nanocomposites with 20, 30, and 40 wt % of both BNNTs and mBNNTs were prepared and denoted as HDPE/BNNT*x* and HDPE/mBNNT*x*, respectively, where *x* represents the BNNT loading. For this, 300 mg of both nanocomposites was prepared as follows: the required amount of BNNTs or mBNNTs was dispersed in xylene with the aid of bath sonication for 15 min. At the same time, the necessary amount of HDPE was dissolved in warm xylene (110 °C) under stirring. Then, the nanotube dispersion was added to the polymer solution, and the mixture was vigorously stirred at 110 °C for 5 h. Subsequently, the mixture was precipitated in 400 mL of methanol, filtered, washed with methanol, and dried at 60 °C under vacuum. The nanocomposites were fabricated into thin films with a nominal thickness of ∼0.5 mm by hot compression using a Collin P-200-P hot press at 160 °C under successive pressure steps. A brass frame, between two flat plates of the same material, was used to control the dimensions and uniform thickness. Neat HDPE was made following the same experimental procedure and used as the control sample.

Characterization. BNNTs before and after functionalization were characterized by Fourier transform infrared (FTIR) spectroscopy on an Agilent Cary 630 FTIR spectrometer, with Diamond attenuated total reflectance (ATR) as the sample interface. Thermogravimetric analysis (TGA) was carried out using a Netzsch TG 209 F1 Iris instrument coupled to a Bruker Tensor 27 FTIR spectrometer. IR data were collected concurrently with the TGA data. Samples of 10 mg were heated from room temperature to 900 °C at a heating rate of 10 °C·min^{-1} under an argon atmosphere. Adsorption and desorption isotherms of water vapor were measured on a dynamic vapor sorption (DVS) system (DVS Advantage Instrument from Surface Measurements Systems) in order to evaluate the changes in water uptake for the hydroxylated BNNTs before and after addressing covalent functionalization. To carry out the experiment, a nanotube film was prepared as follows: 10 mg of nanotubes was dispersed in 25 mL of methanol with the aid of bath sonication for 30 min. Then, the nanotubes were filtered through a polycarbonate membrane, and the resulting nanotube film was left to dry flat at room temperature for 72 h. DVS measurements were performed as follows: 10 mg of the film was dried for 10 h at 70 °C under a dry nitrogen atmosphere. After cooling to 25 °C, the sample was subjected to one cycle of water adsorption and desorption with steps from 0 to 90% of relative humidity. X-ray photoelectron spectroscopy (XPS) data were collected using a Kratos AXIS Ultra delay-line detector (DLD) spectrometer. The instrument was equipped with a hybrid magnetic and electrostatic electron lens system, a DLD, and a monochromatic Al Kα X-ray source (1486.7 eV). Data were collected at a pressure of ∼5 × 10^{-9} Torr with photoelectrons collected at 0° with respect to the sample surface normal. The electron-collection lens aperture was set to sample a 700 × 300 μm spot, and the analyzer pass energy was 160 eV for survey spectra. The binding energy scale was calibrated using C 1s at 284.8 eV, and a charge neutralizer was used because the samples were nonconductive. The XPS data were analyzed using *CasaXPS* software. Every BNNT sample analyzed was in the form of a sheet, which was prepared according to the above-mentioned procedure. The morphology of the BNNT samples was analyzed by SEM (Hitachi, S4700). The SEM samples were prepared by drop-casting a $CHCl_3$ dispersion of the nanotubes onto the SEM pin stub. Transmission electron microscopy (TEM; FEI Titan cubed 80-300) equipped with a Gatan Tridiem 866 image filter, which includes a CCD camera, was used to collect the energy-filtered TEM (EFTEM) imaging. TEM samples were prepared by dispersing a few milligrams of the nanotubes in deionized water using bath sonication for 30 min. A total of 1 drop of the solution was then placed onto a 200 mesh TEM copper grid coated with lacey carbon. SEM images of the nanocomposites were acquired with a Hitachi S8000 scanning electron microscope equipped with a microanalysis Bruker Quantax 200 detector on cryofractured samples from hot-press films coated with a 5 nm gold/palladium layer to avoid sample charging during electron irradiation. The energy-dispersive X-ray (EDX) mapping was performed over the same sample areas for distribution analysis of nanotubes within the polymer matrix.

The degree of crystallinity of all nanocomposites was investigated by differential scanning calorimetry (DSC; PerkinElmer TA C7/DX/DSC7) under a nitrogen atmosphere using samples of ∼6 mg sealed in aluminum pans. Samples were exposed to the following temperature scans: heating to 160 °C at a rate of 10 °C·min^{-1}, holding at this temperature for 3 min to erase thermal history effects, then cooling to 40 °C at a rate of 10 °C·min^{-1}, and finally heating again to 160 °C at a rate of 10 °C·min^{-1}. The degree of crystallinity was obtained by dividing the crystallization or the melting enthalpy (corrected for the amount of HDPE) by the value for 100% crystalline HDPE taken as 286.2 J·g^{-1}.[52]

The thermal conductivity (κ) was calculated using eq 1:

$$\kappa = \rho C_p \alpha \quad (1)$$

where ρ is the density of the materials (estimated by the rule of mixtures, assuming a density of 0.945, 2.29, and 2.13 g·cm^{-3} for HPDE, BNNT, and mBNNT respectively), C_p is the specific heat capacity, and α is the thermal diffusivity. The experimental value of the specific heat capacity (C_p) was estimated by DSC, employing the sapphire methodology described in the ASTM E 1269-01 (see full details in the Supporting Information).

Thermal diffusivity (α) measurements, based on the well-known flash method, were performed with a LFA 447 nanoflash (Netzsch-Gerätebau GmbH). In this method, one side of the sample (∼0.5 mm

DOI: 10.1021/acsanm.8b01992
ACS Appl. Nano Mater. 2019, 2, 440−451

thick) is heated by a short light pulse (xenon flash lamp), and the heat absorbed at the surface is transmitted through the sample and produces a temperature rise on the opposite side. This increase is reflected as a function of time by an IR detector (InSb). The reported values correspond to the average of at least two specimens. Measurements were performed at three temperatures (25, 50, and 75 °C).

RESULTS AND DISCUSSION

The different approaches to graft short PE chains to BNNTs are shown in Scheme 1. It can be seen that the polymer reacts directly with the BNNT walls in the azide strategy, while the strategy based on the Williamson reaction requires prefunctionalization of the hydroxyl groups onto the nanotube surface. FTIR spectroscopy has been employed to determine whether covalent modification of BNNT with PE took place. Figure 1A shows the FTIR spectra of the Williamson reaction product (BNNT-O-PE) and its precursors (PE-Br and BNNT-OH). Moreover, the IR spectrum of the control reaction product has also been included for comparison. The spectrum of BNNT-OH clearly shows the two main peaks associated with the typical vibrations of the BNNT framework, which are the in-plane B−N stretching at 1332 cm^{-1} and the out-of-plane B−N−B bending mode at 771 cm^{-1}. However, the FTIR spectrum of the nanotubes after reaction with PE-Br shows additional features at 2922 and 2849 cm^{-1}, which are assigned to the symmetric and asymmetric stretchings of C−H groups, respectively. The appearance of the new peaks indicates the presence of PE on the nanotube surface but does not provide any evidence for the covalent connection between the polymer and nanotube. However, this ambiguity is resolved by the appearance of a new shoulder feature at 1060 cm^{-1}, which is attributed to the stretching vibration of an ether bond formed after achieving covalent functionalization.[53] To further confirm that the feature at 1060 cm^{-1} is evidence of the covalent formation of the new ether bond, a comparison to the spectrum of the control sample proves out that this feature at 1060 cm^{-1} as well as the stretching vibrations of the C−H groups are fully absent.

Figure 1B shows the FTIR spectra of the reaction product BNNT-N-PE, its precursors, BNNT, the azide-terminated PE, and the control sample. The spectrum for BNNT exhibits the typical B−N stretching and bending modes of BNNTs, at 1355 and 785 cm^{-1}. In the case of the functionalized BNNTs, there are several features that indicate covalent linkage with PE. First, the BNNT-N-PE spectrum also shows these two peaks but slightly shifted to lower wavenumbers, specifically 1340 and 777 cm^{-1}. These shifts are mainly attributed to the covalent bonding of electron-donor groups, in this case nitrene, to the nanotube surface. These groups disrupt the sp^2-bonding network, as previously reported for covalent modification of the nanotube surface with hydroxyl groups.[28] Second, the B−N stretching band is broader in BNNT-N-PE than in BNNT and the control samples, also suggesting the contribution of groups other than those present in the unfunctionalized nanotubes. This broadening can be due to the contribution of the C−N stretching of the pendant group (at 1256 cm^{-1} in the precursor PE-N_3) to the B−N vibration of the nanotube lattice. Third, the very strong band at 2100 cm^{-1}, typical of the azide group, is completely absent in BNNT-N-PE. Last, just like in the spectrum of BNNT-O-PE, the C−H stretching bands are present. Further confirmation of the covalent nature of the PE−BNNT bond is obtained by evaluation of the spectrum of the azide control reaction product. In this spectrum, the typical B−N stretching and bending bands appear at the same wavenumber position as that of the starting material, BNNT. Moreover, the width of the B−N stretching peak is the same as that in the starting material and the C−H stretching vibrations are not observed. Furthermore, the evolution of the IR bands due to the polymer after purification steps, described in detail in Figure S1, also supports the covalent nature of the PE−BNNT bond. Therefore, the IR data provide support for the assertion that PE chains are covalently bound to the surface of the BNNTs.

TGA coupled to a FTIR spectrometer has been employed with the aim of quantifying the amount of polymer attached to the nanotubes. TGA and derivative thermogravimetric (DTG) curves of both the starting materials and reaction products are depicted in Figure 2, along with the FTIR spectra of the products that evolved at 450 °C. As can be seen, the weight remains roughly constant up to 800 °C under an argon atmosphere for neat BNNTs and clearly drops by 1.5 wt % for BNNT-OH (see the inset in Figure 2A). Analysis of the TGA and DTG curves of both reaction products, BNNT-O-PE and BNNT-N-PE, reveals clear similarities between both samples (Figure 2A,B). In both cases, two main events are observed. The first one at about 250 °C can be related to residual solvent molecules that remain physisorbed, as has already been observed for small polar molecules onto BNNT surfaces.[54] In fact, FTIR of evolved gases in this range of temperature shows the presence of a strong carbonyl band coming from DMF (Figure S2). This remaining solvent is easily removed by applying a short thermal treatment (Figure S3). The second weight loss, between 350 and 550 °C, is providing information about the amount of polymer covalently bonded onto the nanotubes. For the BNNT-O-PE sample, a weight loss of 6.5 wt % is measured, while in the case of BNNT-N-PE, it takes a value of 7.3 wt %. The FTIR spectra recorded at 450 °C for both functionalized products confirm that the second weight loss is, in fact, related to the polymer decomposition. Both spectra show the presence of the symmetric and asymmetric vibrations of the C−H bond at 2934−2865 cm^{-1}, which are related to the vibration of the alkyl fragments coming from the polymer degradation.

In accordance with these results, it is confirmed that the azide approach provides a slightly higher degree of functionalization. The grafting densities have roughly been estimated from the TGA results (see full details in the Supporting Information), giving a value of 1 polymer chain per 56 B−N pairs for the BNNT-N-PE sample. This value is much higher than that reported by Sainsbury et al.[36] after carrying out covalent functionalization of h-BN nanosheets with methoxyphenyl carbamate via nitrene chemistry and may be related to an enhanced reactivity of the nanotubes compared to the nanosheets that originated from bond tensions. For the BNNT-O-PE sample, a grafting degree of 1 polymer chain per 66 B−N pairs was determined. In both cases, it may seem like a low level of polymer functionalization, but it is reasonable considering the low reactivity of the nanotube network, which is a key factor limiting the polymer grafting density. Moreover, because the functionalized BNNTs are targeted as polymer fillers, a low degree of functionalization is desirable to preserve the intrinsic properties of the nanotubes as much as possible, while improving their interaction with the polymer matrix.

In addition, elementary analysis was obtained by XPS survey spectra for all relevant species, namely, BNNT-OH, BNNT,

DOI: 10.1021/acsanm.8b01992
ACS Appl. Nano Mater. 2019, 2, 440−451

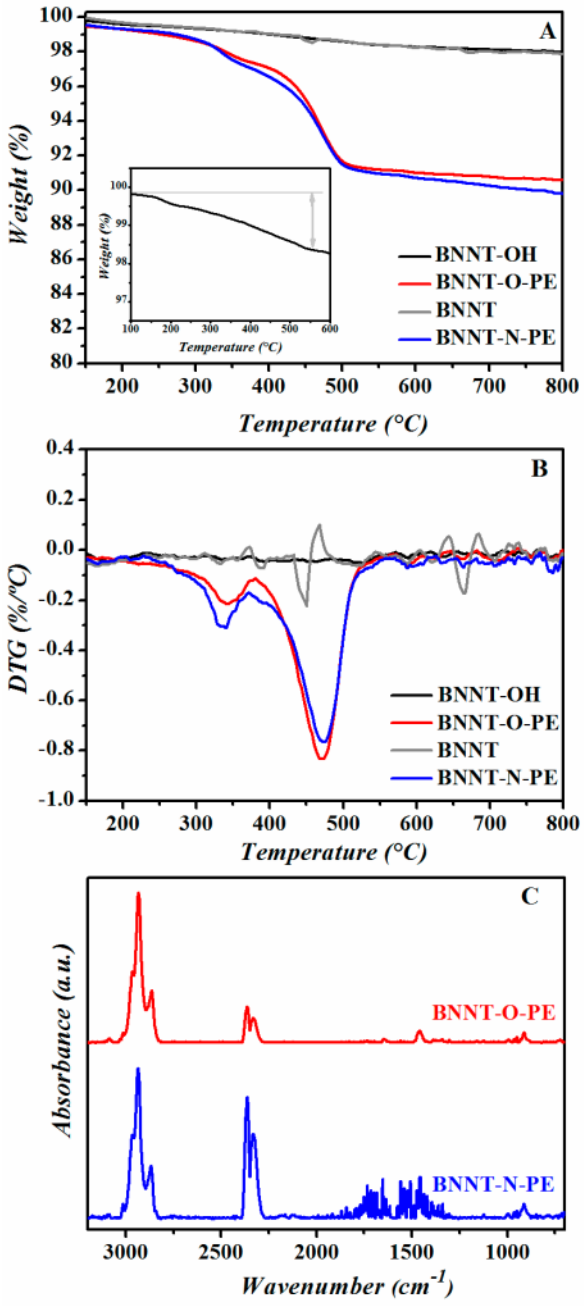

Figure 2. (A) TGA and (B) DTG curves recorded at 10 °C·min^{-1} under an argon atmosphere for both starting nanotubes and both reaction products. The inset in part A shows an enlarged view of the weight loss of the starting BNNT-OH. (C) FTIR spectra recorded at 450 °C for the fragments evolving from the thermal decomposition of both reaction products.

BNNT-O-PE and BNNT-N-PE (Figure S4). Regardless of the strategy used, a carbon content increase of around 15% was observed for the functionalized nanotubes BNNT-O-PE and BNNT-N-PE, compared with their own nanotube precursor. This increase is a significant indication of PE chains remaining in the sample, which can only be realized through the covalent connection without washing away with such intensive cleanup procedures as those described in the Experimental Section. Moreover, bromine was not detected by XPS in the BNNT-O-PE sample, which is additional evidence for the covalent linkage of the PE chains to the nanotube surface; if the carbon content comes from noncovalent PE chains, bromine should be clearly detected because the polymer precursor for the Williamson approach is PE-Br. Therefore, the absence of bromine in the Williamson reaction product supports the covalent functionalization of BNNT-OH with polymer chains. In addition, the unexpected higher level of water uptake from the DVS results (see details in Figure S5) further confirms the covalent nature of the PE/nanotubes for the reaction product BNNT-O-PE. This is because the anchored PE chain on the BNNTs resulted in the debounding of BNNT bundles and led to the unused OH functional groups more available to the surface for water uptake. The XPS results are further supporting this observation.

SEM analysis can offer certain insight for any potential nanotube damage/shortening after chemical functionalization. Figure 3 shows SEM images for both nanotubes and the

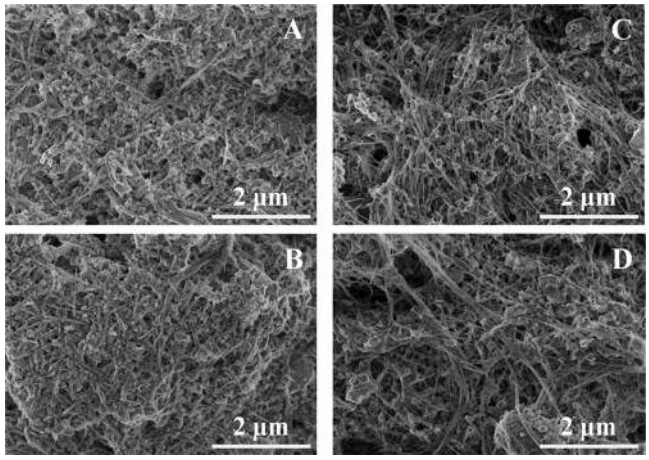

Figure 3. SEM images of BNNT-OH (A), BNNT-O-PE (B), BNNT (C), and BNNT-N-PE (D).

corresponding reaction products. SEM images clearly revealed that the products present morphologies similar to those of their precursors, and no obvious damage or shortening is perceived through the whole surface.

TEM analysis of water-dispersed BNNTs, before and after functionalization by the azide strategy, showed no observable damage to the nanotubes, as seen in Figure 4. This is encouraging because the functionalized BNNTs are proposed to be used as fillers in polymer matrixes, and it is well-known that preserving the structural integrity is essential to maximizing the performance of nanocomposites. From Figure 4B,

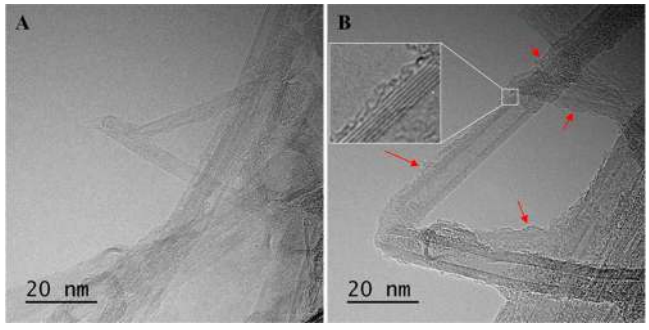

Figure 4. High-resolution TEM images of BNNT (A) and the reaction product BNNT-N-PE (B).

DOI: 10.1021/acsanm.8b01992
ACS Appl. Nano Mater. 2019, 2, 440−451

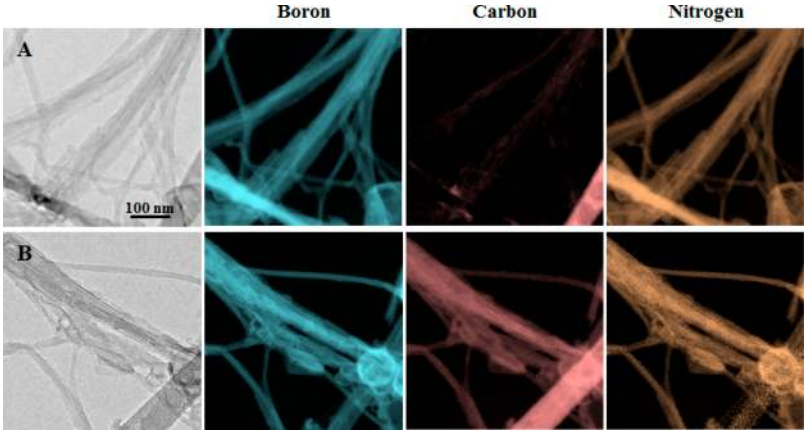

Figure 5. Boron, carbon, and nitrogen elemental maps for BNNTs (A) and BNNT-N-PE (B) obtained by EFTEM.

it can be clearly seen that the functionalized nanotubes are coated by a light polymer sheath (pointed to by red arrows). This finding also supports the success of chemical functionalization of BNNTs with PE chains by the azide approach. Additionally, it should be noted that, despite the direct functionalization of the nanotube surface, the nanotube walls exhibit good crystallinity after the functionalization process, as confirmed in the inset image included in Figure 4B.

Furthermore, boron, carbon and nitrogen elemental maps were obtained for the nanotubes before and after functionalization by EFTEM with the aim of confirming the presence of PE at the surface of BNNT-N-PE. EFTEM imaging is a very efficient technique to assess surface modification of BNNT with polymer chains. Figure 5 compiles the TEM images and elemental maps for each sample. Boron and nitrogen maps are consistent with the expected boron and nitrogen contents for both samples. The most interesting conclusions are obtained when the carbon maps for both samples are compared. Before functionalization, the carbon content is very low (see Figure 5A) and the nanotubes are hardly distinguishable. In contrast, the functionalized nanotubes present a noticeable carbon content uniformly covering the nanotube surface.

INCORPORATION OF BNNTS IN HDPE FOR THERMAL MANAGEMENT

The incorporation of BN materials into polymeric matrixes is an interesting strategy to achieve flexible materials with good thermal conductivity and electrical insulation for heat dissipation.[1] Spectroscopic and TGA results point out that the two synthetic approaches lead to covalent attachment of PE to BNNTs with similar grafting densities. In light of the similar grafting densities obtained by both strategies, the BNNT-N-PE product has been selected to carry out further studies because the reaction is directly conducted on the pristine nanotubes' surface and is simpler in its execution, which makes it more appealing for practical applications. In this study, we conducted an initial assessment about the potential of BNNT-N-PE for thermal management. It is worth mentioning that while the intrinsic thermal conductivity of the BNNTs is expected to decrease with covalent functionalization because of an increase in phonon scattering, the PE moiety covalently attached could improve phonon transfer at the BNNT/HDPE interface, which might overcome the intrinsic thermal conductivity reduction of the filler, as previously proposed,[55] leading to a net improvement of the thermal conductivity.

Both the BNNT-HDPE and mBNNT-HDPE nanocomposites display good flexibility upon bending (insets in Figure 6A,B) in spite of the fact that they contain high amounts of densely packed BNNT nanofillers, as observed by polarized optical microscopy (POM; Figure S6). SEM was employed to better assess the morphology on the cryofractured samples. Figure 6 shows the representative images of both types of nanocomposites at different magnifications. The HDPE/BNNT sample (Figure 6A,C,E) presents some segregation, with regions rich in polymer and others rich in BNNT, while in the case of the HDPE/mBNNT composite, a homogeneous and dense distribution of mBNNT throughout the whole

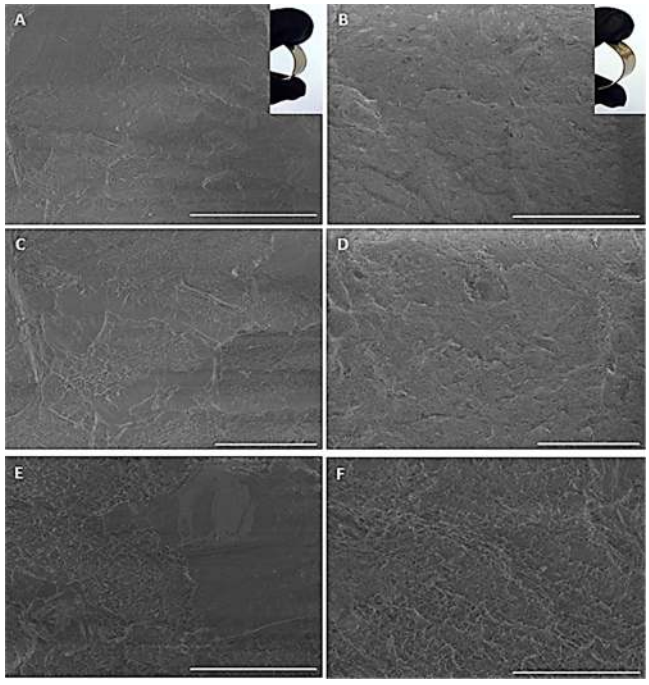

Figure 6. Representative SEM images of HDPE/BNNT40 (A, C, and E) and HDPE/mBNNT40 (B, D, and F) at different magnifications. The scale bars in parts A and B correspond to 50 μm, those in parts C and D to 20 μm, and those in parts E and F to 10 μm. The insets in parts A and B show photographs of HDPE/BNNT40 and HDPE/mBNNT40 films, respectively.

DOI: 10.1021/acsanm.8b01992
ACS Appl. Nano Mater. 2019, 2, 440−451

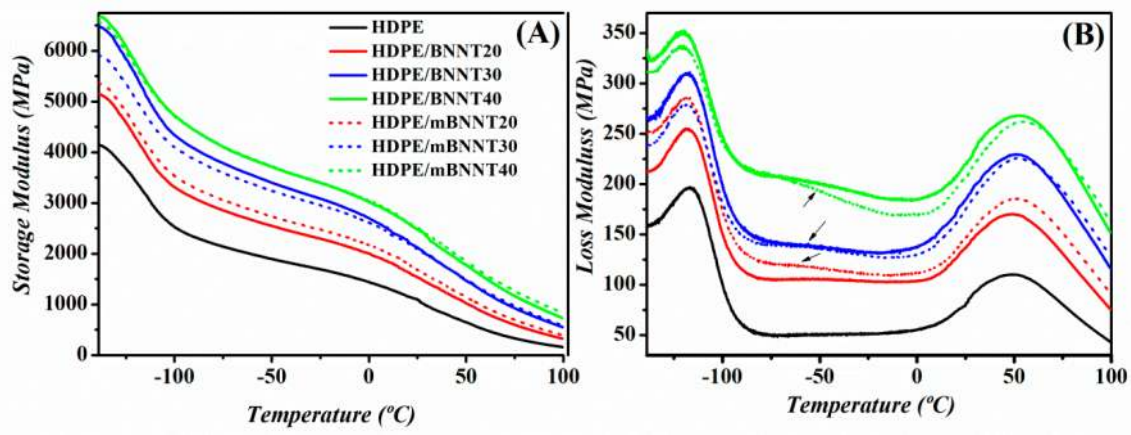

Figure 7. Storage (A) and loss (B) modulus profiles as a function of the temperature for neat HDPE and the nanocomposites. The legend shown in part A applies to both graphs.

analyzed area is observed (Figures 6B,D,F). More SEM analyses are provided in Figures S7 and S8. The EDX mapping for the carbon and nitrogen elements (Figure S9) further confirmed a better distribution of mBNNT than BNNT in the composites.

In addition to the morphology changes described above, DSC studies were also carried out in order to study the influence of the nanotube filler on the microstructure of the polymer matrix. A decrease of crystallinity of HDPE in the nanocomposites with increasing amount of nanotubes was observed regardless of their types and attributed to a reduction in the polymer mobility (Figure S10 and Table S1). With an increase of the nanotubes content, the entanglement between the nanotubes and polymer chains significantly increases, which limited the assembly of polymer chains to form crystallites.

The effects of the BNNT nature (pristine or modified) and their content on the mechanical properties of HDPE nanocomposites were evaluated by dynamic mechanical analysis (DMA). Variation of the storage modulus (E') as a function of the temperature for HDPE and its nanocomposites is shown in Figure 7A. A significant increase in the storage modulus of HDPE with the incorporation of the nanofiller was clearly observed at all temperatures because of a reinforcing effect of BNNTs. In addition, at low filler content (20 wt %), the mBNNT-HDPE nanocomposites present a higher modulus compared with the unmodified one, which can be attributed to a superior interfacial adhesion and a homogeneous dispersion of the nanofillers into the matrix. However, as the filler loading increases, the modulus values of both nanocomposites tend to become similar.

DMA also provides information about the mobility of the polymer chains, and it is a very useful tool to investigate the interfacial behavior in nanocomposites. Figure 7B represents variation of the loss modulus (E') as a function of the temperature for HDPE and its nanocomposites. HDPE shows two relaxation peaks: at −112.5 °C in the range of −150 to −100 °C and at 49 °C in the range of 0−65 °C, which are assigned to γ and α relaxations, respectively. Linear and branched PE, as well as copolymers of ethylene, display a series of transitions below the melting temperature that have been conventionally designated as α, β, and γ relaxations in order of decreasing temperature.[56,57] It is generally accepted that the α relaxation is related to the motions of the chain units that lie within the crystalline region of the polymer and occur in the temperature range of 0−65 °C. The temperature at the maximum of the α relaxation shifts to higher values for the nanocomposites, with the effect being more pronounced when mBNNT is used. The γ relaxation is from the amorphous phase and more specifically from the crankshaft movement of four methylene groups within this phase and can be considered to be the glass transition temperature of HDPE. With the incorporation of nanotubes, the nanocomposites show an additional relaxation in the temperature range of −75 to 0 °C (arrows in Figure 7B), which can be related to the interface between the matrix and nanofillers. This transition is more relevant for the nanocomposites with modified BNNTs, and the effect increases with the mBNNT content, corroborating the influence of functionalization of the nanomaterial on the interfacial properties. The appearance of a similar relaxation in the HDPE nanocomposites was previously reported in composites filled with Al_2O_3 fibers.[58]

In order to further confirm the development of a stronger polymer/filler interface when mBNNT is used, the coefficient of reinforcement (C parameter) has been calculated from the DMA results.[59−61] The "C" parameter provides an estimation of the effectiveness of the type of filler and can be calculated using eq 2:

$$C = \frac{\left(\frac{E_g'}{E_r'}\right)_{\text{nanocomposite}}}{\left(\frac{E_g'}{E_r'}\right)_{\text{polymer}}} \quad (2)$$

where E_r' and E_g' are the values of the storage modulus that correspond to the rubbery (40 °C) and glassy (−115 °C) regions, respectively. The "C" parameter is a relative measure of the reduction in the modulus when the temperature rises and the material passes through its glass transition. Its value is inversely proportional to the effectiveness of the filler in the polymer matrix.[59] Consequently, the lower the "C" parameter, the more effective the filler is. The values obtained for the different HDPE nanocomposites are given in Table 1. An increase of the filler loading leads to a decrease in the "C" parameter, and for the same composition, the "C" value is always lower when mBNNTs are used. These results highlight the enhanced efficiency of mBNNT within the HDPE matrix,

DOI: 10.1021/acsanm.8b01992
ACS Appl. Nano Mater. 2019, 2, 440−451

Table 1. "C" Parameter for the HDPE Nanocomposites Estimated from the DMA Results

sample	E_r' (GPa)	E_g' (GPa)	"C" parameter
HDPE	0.8	3.2	
HDPE/BNNT20	1.2	4.0	0.83
HDPE/BNNT30	1.7	5.2	0.75
HDPE/BNNT40	2.0	5.4	0.68
HDPE/mBNNT20	1.4	4.2	0.79
HDPE/mBNNT30	1.7	4.8	0.70
HDPE/mBNNT40	2.1	5.4	0.64

which is related to the increased filler/polymer affinity derived from the chemical functionalization of the nanotubes.

To examine the influence of the better distribution of the nanotubes in the HDPE matrix and the interfacial interaction improvement, the thermal conductivities (κ) of the HDPE/BNNT and HDPE/mBNNT samples with different filler loadings have been measured. Figure 8A shows variation of κ with the filler loading for both types of nanocomposites at room temperature. It is evident that the κ value of the nanocomposites is much higher than that of pure HDPE because of the presence of nanotubes, with nanocomposites containing mBNNT displaying the highest values. In addition, a different variation of κ with the filler loading is observed for the different types of fillers. While at low filler loadings both materials present similar values, at higher loadings the nanocomposites with mBNNT present superior κ (Figure 8A). This is attributed to the better distribution of mBNNT, as observed in SEM/EDX experiments, and/or to changes in the polymer microstructure, as demonstrated by DSC and DMA, leading to a decrease on the filler/polymer thermal interface resistance because of covalent attachment of the filler to the matrix. Nevertheless, even without covalent attachment, as in the case with pristine BNNT, a conductive pathway is formed (Figure S8) that causes the thermal conductivity to increase.

In order to shed light on the different behaviors demonstrated from both nanocomposites, modeling to predict κ was carried out. The application of these models requires the estimation of the filler content in the volume percentage in each nanocomposite, which has been estimated considering the densities of HPDE, BNNT, and mBNNT as 0.985, 2.29, and 2.13 g·cm^{-3}, respectively. A widely known effective medium theory (EMT),[5,62] which considers spherical particles dispersed in a continuous medium and has been valid for the volume fractions used in this study (below 25%), was initially explored. However, this EMT model (Figure 8B) does not fit the experimental data in any of the two types of nanocomposites probably because it ignores the interaction between the filler particles. The model proposed by Agari and Uno[63] takes into account aspects related to the crystallinity and crystal size of a polymer and the ease of forming a thermal conductive path of fillers, with the latter being associated with the dispersion state of the filler. Variation for the thermal conductivity in this model is described by eq 3:

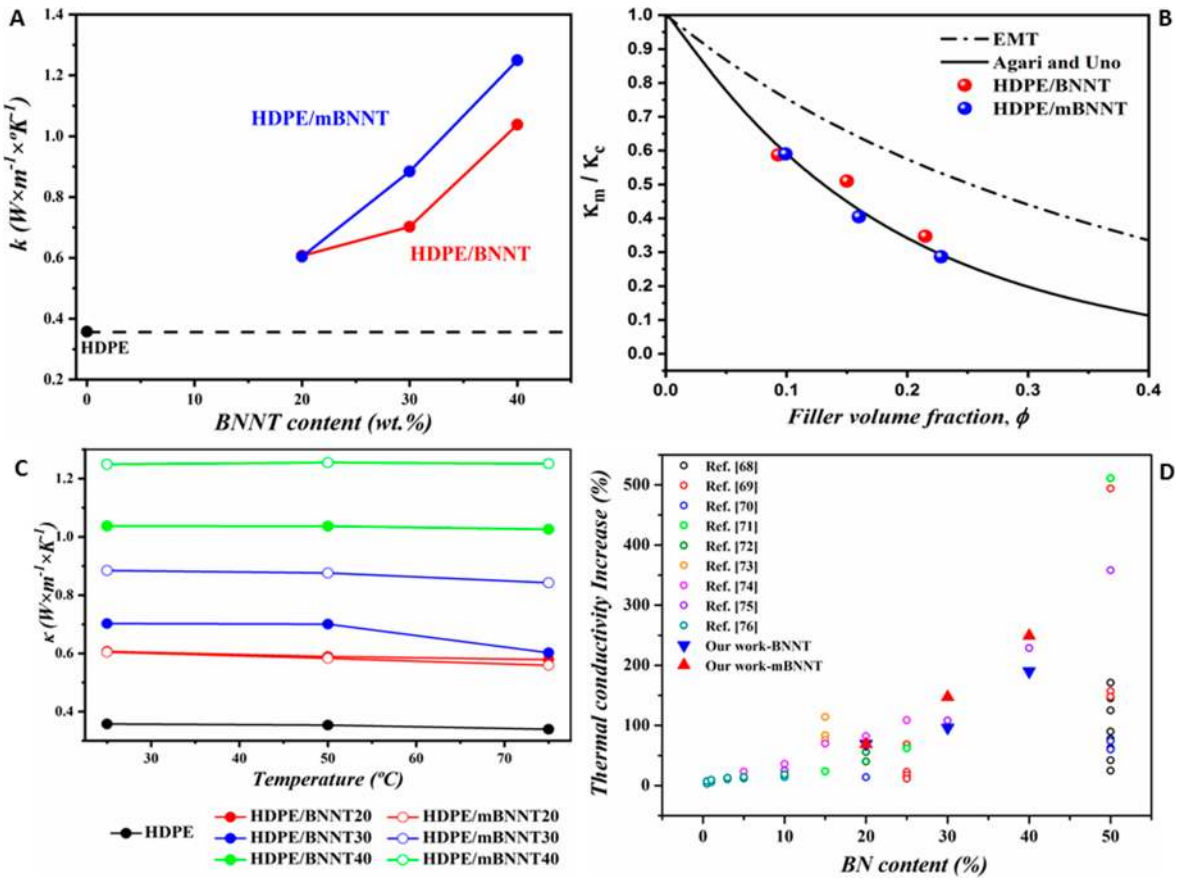

Figure 8. Evaluation of the changes in the thermal conductivity of the nanocomposites prepared in this study. (A) Variation with the filler loading. (B) Comparison of the experimental results with the prediction models. (C) Variation with the temperature. (D) Comparison with data reported in the literature.[68−76]

DOI: 10.1021/acsanm.8b01992
ACS Appl. Nano Mater. 2019, 2, 440−451

$$\log k_c = \phi C_2 \log k_f + (1 - \phi) \log(C_1 k_m) \quad (3)$$

where k_c, k_f, and k_m are the thermal conductivities of the nanocomposite, filler, and matrix, respectively, ϕ is the filler volume fraction, C_1 is a factor related to the crystallinity, and C_2 to the ease of forming of the conductive path. In order to fit the experimental data, we fixed one parameter and varied the other. First, considering the literature data,[64] we selected $C_1 = 1$ and $0.6 \leq C_2 \leq 0.9$, obtaining the best fitting for all compositions of HDPE/mBNNT when $C_2 = 0.75$ (Figures 8B and S11A). For HDPE/BNNT, the behavior seems more complex because it cannot be adjusted. At low filler loading, it takes similar values to the HDPE/mBNNT nanocomposite, but at higher loadings, the experimental points seem to be better fitted with lower values of C_2 (Figure S11A). This confirms the results of SEM in which a better distribution of mBNNT along the HDPE matrix is observed. At low filler concentrations, both nanocomposites behave similarly. However, at higher loadings, achieving a homogeneous distribution of the filler is more difficult and the formation of the conductive path throughout the matrix is favored by chemical modification. Additionally, we intended to fit the data for HDPE/BNNT, fixing $C_2 = 0.75$ and giving C_1 common values for PE,[64] so that $0.8 \leq C_1 \leq 0.9$ (Figure S11B). Except at the lowest concentration, the experimental data are well adjusted with the curve traced for $C_1 = 0.8$, the lowest tested value. This suggests that the microstructure can also affect the thermal conductivity in this nanocomposite where the filler is not optimally dispersed. This is a very interesting feature that has to be confirmed and will be addressed in ongoing studies.

The dependence of the thermal conductivity on the temperature was also evaluated. Both nanocomposites displayed good stability of the thermal conductivity with the temperature (Figure 8C). This might be due to a counterbalance between a decrease in the interfacial resistance (increase of the thermal conductivity) and other factors such as the disorder induced in crystalline polymers,[43] phonon−phonon scattering[44] and/or Umklapp phonon scattering[65] in BNNT,[66] and mismatch between the thermal expansion coefficient of HDPE (ca. 150 ppm·°C^{-1}) and BN (ca. 1 ppm·°C^{-1})[67] (which causes a decrease in the thermal conductivity with the temperature). These results are of relevance for applications that require relatively high operating temperatures.

To evaluate the scope and potential of the approach proposed in this study, the results obtained have been compared with previous results of HDPE/BN composites in the literature. In Figure 8D, it can be seen that the improvement in the thermal conductivity obtained in this study with mBNNT exceeds those previously reported with the same filler loading. Moreover, the use of higher filler loadings (up to 50 wt %) caused different effects on the thermal conductivity.[68−71,75]

CONCLUSIONS

The covalently chemical functionalization of BNNTs with PE chains is achieved for the first time through two different "grafting-to" approaches. Chemical functionalization is confirmed using TGA, FTIR, XPS, DVS and TEM. A functionalization degree in the range of ∼7 wt % is obtained from the two approaches. The product from the azide strategy is selected as the filler for HDPE because the reaction is directly conducted on the nanotube surface, avoiding the time-consuming and costly prefunctionalization steps. This level of functionalization provides excellent compatibility with the HDPE matrix while maintaining the integrity of the nanotubes. The enhanced compatibility leads to a better transfer of properties from the nanotubes to the matrix. In particular, we demonstrate significant enhancement of the storage modulus and thermal properties over unfunctionalized composites. Variation of the thermal conductivity of nanocomposites with the concentration of mBNNT is perfectly adjusted with the model of Agari and Uno using common values for the parameters related to the crystallinity and ease of formation of the conductive path, previously reported for PE.

The strategies described here pave the way to cheap, lightweight flexible, and thermal-conductive nanocomposite materials for heat-transfer applications.

ASSOCIATED CONTENT

Supporting Information

The Supporting Information is available free of charge on the ACS Publications website at DOI: 10.1021/acsanm.8b01992.

FTIR, XPS, TGA-IR, and DVS of modified BNNTs and POM, SEM, EDX, DSC, and thermal conductivity modeling of HDPE/BNNT nanocomposites (PDF)

AUTHOR INFORMATION

Corresponding Author

*E-mail: horacio@ictp.csic.es (H.J.S.).

ORCID

Yadienka Martínez-Rubí: 0000-0002-1548-6504

Horacio J. Salavagione: 0000-0001-9588-7879

Notes

The authors declare no competing financial interest.

ACKNOWLEDGMENTS

Financial support from Spain (Grants MAT2013-47898-C2-2-R and MAT2017-88382-P) and CSIC (Grant 201760I084) is gratefully acknowledged. S.Q.-D. acknowledges MINEICO for the FPI Fellowship and for a grant under the Predoctoral Mobility Program (EEBB-I-17-12247) and the hospitality of the National Research Council Canada (NRC). The authors are indebted to Malgorzata Daroszewska for the TGA and DVS measurements, to Gordon Chan for recording the SEM images of the nanotubes, to Oltion Kodra for taking the XPS measurements, to Prof. Luis Barral from University of Coruña for his help with the thermal conductivity measurements, to Prof. Rosario Benavente (ICTP-CSIC) for her help with the Cp and POM measurements, and to David Gómez of the Characterization Service of the Institute of Polymer Science & Technology for his assistance in the SEM/EDX measurements of nanocomposites. This work was partly supported by the Security Materials Technologies Program of the NRC (Grant A1-9469).

REFERENCES

(1) Xu, X.; Chen, J.; Zhou, J.; Li, B. Thermal Conductivity of Polymers and Their Nanocomposites. *Adv. Mater.* **2018**, *30*, 1705544.

(2) Li, Q.; Chen, L.; Gadinski, M. R.; Zhang, S.; Zhang, G.; Li, H. U.; Iagodkine, E.; Haque, A.; Chen, L.-Q.; Jackson, T. N.; Wang, Q. Flexible High-Temperature Dielectric Materials from Polymer Nanocomposites. *Nature* **2015**, *523*, 576−579.

(3) Song, W.-L.; Wang, P.; Cao, L.; Anderson, A.; Meziani, M. J.; Farr, A. J.; Sun, Y.-P. Polymer/Boron Nitride Nanocomposite

DOI: 10.1021/acsanm.8b01992
ACS Appl. Nano Mater. 2019, 2, 440−451

Materials for Superior Thermal Transport Performance. *Angew. Chem., Int. Ed.* **2012**, *51*, 6498−6501.
(4) Yang, X.; Liang, C.; Ma, T.; Guo, Y.; Kong, J.; Gu, J.; Chen, M.; Zhu, J. A Review on Thermally Conductive Polymeric Composites: Classification, Measurement, Model and Equations, Mechanism and Fabrication Methods. *Adv. Compos. Hybrid Mater.* **2018**, *1*, 207−230.
(5) Mehra, N.; Mu, L.; Ji, T.; Yang, X.; Kong, J.; Gu, J.; Zhu, J. Thermal Transport in Polymeric Materials and across Composite Interfaces. *Appl. Mater. Today* **2018**, *12*, 92−130.
(6) Li, Y.; Xu, G.; Guo, Y.; Ma, T.; Zhong, X.; Zhang, Q.; Gu, J. Fabrication, Proposed Model and Simulation Predictions on Thermally Conductive Hybrid Cyanate Ester Composites with Boron Nitride Fillers. *Composites, Part A* **2018**, *107*, 570−578.
(7) Yang, X.; Tang, L.; Guo, Y.; Liang, C.; Zhang, Q.; Kou, K.; Gu, J. Improvement of Thermal Conductivities for PPS Dielectric Nanocomposites via Incorporating NH_2-POSS Functionalized *n*BN Fillers. *Composites, Part A* **2017**, *101*, 237−242.
(8) Gu, J.; Liang, C.; Dang, J.; Dong, W.; Zhang, Q. Ideal Dielectric Thermally Conductive Bismaleimide Nanocomposites Filled with Polyhedral Oligomeric Silsesquioxane Functionalized Nanosized Boron Nitride. *RSC Adv.* **2016**, *6*, 35809−35814.
(9) Gu, J.; Xu, S.; Zhuang, Q.; Tang, Y.; Kong, J. Hyperbranched Polyborosilazane and Boron Nitride Modified Cyanate Ester Composite with Low Dielectric Loss and Desirable Thermal Conductivity. *IEEE Trans. Dielectr. Electr. Insul.* **2017**, *24*, 784−790.
(10) Li, L.; Li, L. H.; Ramakrishnan, S.; Dai, X. J.; Nicholas, K.; Chen, Y.; Chen, Z.; Liu, X. Controlling Wettability of Boron Nitride Nanotube Films and Improved Cell Proliferation. *J. Phys. Chem. C* **2012**, *116*, 18334−18339.
(11) Wang, J.; Lee, C. H.; Yap, Y. K. Recent Advancements in Boron Nitride Nanotubes. *Nanoscale* **2010**, *2*, 2028−2034.
(12) Kim, K. S.; Kingston, C. T.; Hrdina, A.; Jakubinek, M. B.; Guan, J.; Plunkett, M.; Simard, B. Hydrogen-Catalyzed, Pilot-Scale Production of Small-Diameter Boron Nitride Nanotubes and Their Macroscopic Assemblies. *ACS Nano* **2014**, *8*, 6211−6220.
(13) Fathalizadeh, A.; Pham, T.; Mickelson, W.; Zettl, A. Scaled Synthesis of Boron Nitride Nanotubes, Nanoribbons and Nanococoons Using Direct Feedstock Injection into an Extended-Pressure, Inductively-Coupled Thermal Plasma. *Nano Lett.* **2014**, *14*, 4881−4886.
(14) Smith, M. W.; Jordan, K. C.; Park, C.; Kim, J.-W.; Lillehei, P. T.; Crooks, R.; Harrison, J. S. Very Long Single- and Few-Walled Boron Nitride Nanotubes via the Pressurized Vapor/Condenser Method. *Nanotechnology* **2009**, *20*, 505604.
(15) Jakubinek, M. B.; Niven, J. F.; Johnson, M. B.; Ashrafi, B.; Kim, K. S.; Simard, B.; White, M. A. Thermal Conductivity of Bulk Boron Nitride Nanotube Sheets and Their Epoxy-Impregnated Composites. *Phys. Status Solidi A* **2016**, *213*, 2237−2242.
(16) Kim, K. S.; Jakubinek, M. B.; Martinez-Rubi, Y.; Ashrafi, B.; Guan, J.; O'Neill, K.; Plunkett, M.; Hrdina, A.; Lin, S.; Dénommée, S.; Kingston, C.; Simard, B. Polymer Nanocomposites from Free-Standing, Macroscopic Boron Nitride Nanotube Assemblies. *RSC Adv.* **2015**, *5*, 41186−41192.
(17) Jakubinek, M. B.; Ashrafi, B.; Zhang, Y.; Martinez-Rubi, Y.; Kingston, C. T.; Johnston, A.; Simard, B. Single-Walled Carbon Nanotube-Epoxy Composites for Structural and Conductive Aerospace Adhesives. *Composites, Part B* **2015**, *69*, 87−93.
(18) Zhi, C.; Bando, Y.; Terao, T.; Tang, C.; Kuwahara, H.; Golberg, D. Towards Thermoconductive, Electrically Insulating Polymeric Composites with Boron Nitride Nanotubes as Fillers. *Adv. Funct. Mater.* **2009**, *19*, 1857−1862.
(19) Zhi, C.; Bando, Y.; Tang, C.; Honda, S.; Kuwahara, H.; Golberg, D. Boron Nitride Nanotubes/Polystyrene Composites. *J. Mater. Res.* **2006**, *21*, 2794−2800.
(20) Meng, W.; Huang, Y.; Fu, Y.; Wang, Z.; Zhi, C. Polymer Composites of Boron Nitride Nanotubes and Nanosheets. *J. Mater. Chem. C* **2014**, *2*, 10049−10061.
(21) Zhi, C. Y.; Bando, Y.; Terao, T.; Tang, C. C.; Kuwahara, H.; Golberg, D. Chemically Activated Boron Nitride Nanotubes. *Chem. - Asian J.* **2009**, *4*, 1536−1540.
(22) Li, L.; Chen, Y.; Stachurski, Z. H. Boron Nitride Nanotube Reinforced Polyurethane Composites. *Prog. Nat. Sci.* **2013**, *23*, 170−173.
(23) Tasis, D.; Tagmatarchis, N.; Bianco, A.; Prato, M. Chemistry of Carbon Nanotubes. *Chem. Rev.* **2006**, *106*, 1105−1136.
(24) Homenick, C. M.; Lawson, G.; Adronov, A. Polymer Grafting of Carbon Nanotubes Using Living Free Radical Polymerization. *Polym. Rev.* **2007**, *47*, 265−290.
(25) Chopra, N. G.; Luyken, R. J.; Cherrey, K.; Crespi, V. H.; Cohen, M. L.; Louie, S. G.; Zettl, A. Boron Nitride Nanotubes. *Science* **1995**, *269*, 966−967.
(26) Golberg, D.; Bando, Y.; Huang, Y.; Terao, T.; Mitome, M.; Tang, C.; Zhi, C. Boron Nitride Nanotubes and Nanosheets. *ACS Nano* **2010**, *4*, 2979−2993.
(27) Shin, H.; Guan, J.; Zgierski, M. Z.; Kim, K. S.; Kingston, C. T.; Simard, B. Covalent Functionalization of Boron Nitride Nanotubes via Reduction Chemistry. *ACS Nano* **2015**, *9*, 12573−12582.
(28) Lin, S.; Ashrafi, B.; Laqua, K.; Su Kim, K.; Simard, B. Covalent Derivatization of Boron Nitride Nanotubes with Peroxides and Their Application in Polycarbonate Composites. *New J. Chem.* **2017**, *41*, 7571−7577.
(29) Ciofani, G.; Genchi, G. G.; Liakos, I.; Athanassiou, A.; Dinucci, D.; Chiellini, F.; Mattoli, V. A Simple Approach to Covalent Functionalization of Boron Nitride Nanotubes. *J. Colloid Interface Sci.* **2012**, *374*, 308−314.
(30) Zhou, S.-J.; Ma, C.-Y.; Meng, Y.-Y.; Su, H.-F.; Zhu, Z.; Deng, S.-L.; Xie, S.-Y. Activation of Boron Nitride Nanotubes and Their Polymer Composites for Improving Mechanical Performance. *Nanotechnology* **2012**, *23*, 55708.
(31) Li, Y.; Peng, Z.; Larios, E.; Wang, G.; Lin, J.; Yan, Z.; Ruiz-Zepeda, F.; José-Yacamán, M.; Tour, J. M. Rebar Graphene from Functionalized Boron Nitride Nanotubes. *ACS Nano* **2015**, *9*, 532−538.
(32) Sainsbury, T.; Ikuno, T.; Okawa, D.; Pacilé, D.; Fréchet, J. M. J.; Zettl, A. Self-Assembly of Gold Nanoparticles at the Surface of Amine- and Thiol-Functionalized Boron Nitride Nanotubes. *J. Phys. Chem. C* **2007**, *111*, 12992−12999.
(33) Zhi, C.; Bando, Y.; Tang, C.; Honda, S.; Sato, K.; Kuwahara, H.; Golberg, D. Covalent Functionalization: Towards Soluble Multiwalled Boron Nitride Nanotubes. *Angew. Chem., Int. Ed.* **2005**, *44*, 7932−7935.
(34) Sainsbury, T.; O'Neill, A.; Passarelli, M. K.; Seraffon, M.; Gohil, D.; Gnaniah, S.; Spencer, S. J.; Rae, A.; Coleman, J. N. Dibromocarbene Functionalization of Boron Nitride Nanosheets: Toward Band Gap Manipulation and Nanocomposite Applications. *Chem. Mater.* **2014**, *26*, 7039−7050.
(35) Sainsbury, T.; Satti, A.; May, P.; Wang, Z. M.; McGovern, I.; Gun'ko, Y. K.; Coleman, J. Oxygen Radical Functionalization of Boron Nitride Nanosheets. *J. Am. Chem. Soc.* **2012**, *134*, 18758−18771.
(36) Sainsbury, T.; Satti, A.; May, P.; O'Neill, A.; Nicolosi, V.; Gun'ko, Y. K.; Coleman, J. N. Covalently Functionalized Hexagonal Boron Nitride Nanosheets by Nitrene Addition. *Chem. - Eur. J.* **2012**, *18*, 10808−10812.
(37) Flores, A.; Ania, F.; Salavagione, H. J.; Ellis, G.; Saurel, D.; Gómez-Fatou, M. A. Local Mechanical Properties of Graphene/Polyethylene-Based Nanocomposites by Depth-Sensing Indentation. *Eur. Polym. J.* **2016**, *74*, 120−129.
(38) Castelaín, M.; Martínez, G.; Marco, C.; Ellis, G.; Salavagione, H. J. Effect of Click-Chemistry Approaches for Graphene Modification on the Electrical, Thermal, and Mechanical Properties of Polyethylene/Graphene Nanocomposites. *Macromolecules* **2013**, *46*, 8980−8987.
(39) Quiles-Díaz, S.; Enrique-Jimenez, P.; Papageorgiou, D. G.; Ania, F.; Flores, A.; Kinloch, I. A.; Gómez-Fatou, M. A.; Young, R. J.; Salavagione, H. J. Influence of the Chemical Functionalization of

DOI: 10.1021/acsanm.8b01992
ACS Appl. Nano Mater. 2019, 2, 440−451

Graphene on the Properties of Polypropylene-Based Nanocomposites. *Composites, Part A* **2017**, *100*, 31−39.
(40) Enrique-Jimenez, P.; Quiles-Díaz, S.; Salavagione, H. J.; Wesner, D.; Schönherr, H.; González-Casablanca, J.; García-Quismondo, R.; Martínez, G.; Gómez-Fatou, M. A.; Ania, F.; Flores, A. Control of the Structure and Properties of SEBS Nanocomposites via Chemical Modification of Graphene with Polymer Brushes. *Eur. Polym. J.* **2017**, *97*, 1−13.
(41) Salavagione, H. J.; Quiles-Díaz, S.; Enrique-Jimenez, P.; Martínez, G.; Ania, F.; Flores, A.; Gómez-Fatou, M. A. Development of Advanced Elastomeric Conductive Nanocomposites by Selective Chemical Affinity of Modified Graphene. *Macromolecules* **2016**, *49*, 4948−4956.
(42) Yu, J.; Mo, H.; Jiang, P. Polymer/Boron Nitride Nanosheet Composite with High Thermal Conductivity and Sufficient Dielectric Strength. *Polym. Adv. Technol.* **2015**, *26*, 514−520.
(43) Lee, J.; Jung, H.; Yu, S.; Man Cho, S.; Tiwari, V. K.; Babu Velusamy, D.; Park, C. Boron Nitride Nanosheets (BNNSs) Chemically Modified by "Grafting-From" Polymerization of Poly(caprolactone) for Thermally Conductive Polymer Composites. *Chem. - Asian J.* **2016**, *11*, 1921−1928.
(44) Ejaz, M.; Rai, S. C.; Wang, K.; Zhang, K.; Zhou, W.; Grayson, S. M. Surface-Initiated Atom Transfer Radical Polymerization of Glycidyl Methacrylate and Styrene from Boron Nitride Nanotubes. *J. Mater. Chem. C* **2014**, *2*, 4073−4079.
(45) Cui, Z.; Martinez, A. P.; Adamson, D. H. PMMA Functionalized Boron Nitride Sheets as Nanofillers. *Nanoscale* **2015**, *7*, 10193−10197.
(46) Rubio, N.; Au, H.; Leese, H. S.; Hu, S.; Clancy, A. J.; Shaffer, M. S. P. Grafting from versus Grafting to Approaches for the Functionalization of Graphene Nanoplatelets with Poly(Methyl Methacrylate). *Macromolecules* **2017**, *50*, 7070−7079.
(47) Ye, Y. S.; Chen, Y. N.; Wang, J. S.; Rick, J.; Huang, Y. J.; Chang, F. C.; Hwang, B. J. Versatile Grafting Approaches to Functionalizing Individually Dispersed Graphene Nanosheets Using RAFT Polymerization and Click Chemistry. *Chem. Mater.* **2012**, *24*, 2987−2997.
(48) Vollhardt, P.; Schore, N. *Organic Chemistry: Structure and Function*; W. H. Freeman and Company, 2015.
(49) Simard, B.; Ingold, K.; Walker, S.; Iannitto, R.; Cho, H.; Martinez-Rubi, Y.; Kim, K. S.; Kingston, C. T.; Dénommée, S.; Ruth, D.; Plunket, M. Process and Apparatus for Purifying BNNT. U.S. Provisional Patent Application 62/696,377, 2018.
(50) Guan, J. W.; Kim, K. S.; Jakubinek, M. B.; Simard, B. pH-Switchable Water-soluble Boron Nitride Nanotubes. *ChemistrySelect* **2018**, *3*, 9308−9312.
(51) Guan, J.; Ashrafi, B.; Martinez-Rubi, Y.; Jakubinek, M. B.; Rahmat, M.; Kim, K. S.; Simard, B. Epoxy Resin Nanocomposites with Hydroxyl (OH) and Amino (NH_2) Functionalized Boron Nitride Nanotubes. *Nanocomposites* **2018**, *4*, 10−17.
(52) Wunderlich, B.; Cormier, C. M. Heat of Fusion of Polyethylene. *J. Polym. Sci. Part A-2 Polym. Phys.* **1967**, *5*, 987−988.
(53) Colthup, N. B.; Daly, L. H.; Wiberley, S. E. *Introduction to Infrared and Raman Spectroscopy*; Academic Press, 1990.
(54) Rimola, A.; Sodupe, M. Physisorption vs. Chemisorption of Probe Molecules on Boron Nitride Nanomaterials: The Effect of Surface Curvature. *Phys. Chem. Chem. Phys.* **2013**, *15*, 13190−13198.
(55) Burger, N.; Laachachi, A.; Ferriol, M.; Lutz, M.; Toniazzo, V.; Ruch, D. Review of Thermal Conductivity in Composites: Mechanisms, Parameters and Theory. *Prog. Polym. Sci.* **2016**, *61*, 1−28.
(56) Laredo, E.; Suarez, N.; Bello, A.; Rojas de Gáscue, B.; Gomez, M. A.; Fatou, J. M. G. α, β and γ Relaxations of Functionalized HD Polyethylene: A TSDC and a Mechanical Study. *Polymer* **1999**, *40*, 6405−6416.
(57) Nielsen, L. E. *Mechanical Properties of Polymers and Composites*; Marcel Dekker: New York , 1974.
(58) Zhang, S.; Ke, Y.; Cao, X.; Ma, Y.; Wang, F. Effect of Al_2O_3 Fibers on the Thermal Conductivity and Mechanical Properties of High Density Polyethylene with the Absence and Presence of Compatibilizer. *J. Appl. Polym. Sci.* **2011**, *124*, 4874−4881.
(59) Singh, V. P.; K. K, V.; Sharma, S.; Kapur, G. S.; Choudhary, V. Polyethylene/Sepiolite Clay Nanocomposites: Effect of Clay Content, Compatibilizer Polarity, and Molar Mass on Viscoelastic and Dynamic Mechanical Properties. *J. Appl. Polym. Sci.* **2017**, *134*, 45197.
(60) Jyoti, J.; Singh, B. P.; Arya, A. K.; Dhakate, S. R. Dynamic Mechanical Properties of Multiwall Carbon Nanotube Reinforced ABS Composites and Their Correlation with Entanglement Density, Adhesion, Reinforcement and C Factor. *RSC Adv.* **2016**, *6*, 3997−4006.
(61) Chauhan, S. S.; Singh, B. P.; Malik, R. S.; Verma, P.; Choudhary, V. Detailed Dynamic Mechanical Analysis of Thermo-mechanically Stable Melt-Processed PEK-MWCNT Nanocomposites. *Polym. Compos.* **2018**, *39*, 2587−2596.
(62) Nan, C.-W.; Birringer, R.; Clarke, D. R.; Gleiter, H. Effective Thermal Conductivity of Particulate Composites with Interfacial Thermal Resistance. *J. Appl. Phys.* **1997**, *81*, 6692−6699.
(63) Agari, Y.; Uno, T. Estimation on Thermal Conductivities of Filled Polymers. *J. Appl. Polym. Sci.* **1986**, *32*, 5705−5712.
(64) Agari, Y.; Ueda, A.; Nagai, S. Thermal Conductivity of a Polymer Composite. *J. Appl. Polym. Sci.* **1993**, *49*, 1625−1634.
(65) Balandin, A. A. Thermal Properties of Graphene and Nanostructured Carbon Materials. *Nat. Mater.* **2011**, *10*, 569−581.
(66) Lindsay, L.; Broido, D. A. Theory of Thermal Transport in Multilayer Hexagonal Boron Nitride and Nanotubes. *Phys. Rev. B: Condens. Matter Mater. Phys.* **2012**, *85*, 35436.
(67) Zhou, W. Thermal and Dielectric Properties of the AlN Particles Reinforced Linear Low-Density Polyethylene Composites. *Thermochim. Acta* **2011**, *512*, 183−188.
(68) Zhang, X.; Wu, H.; Guo, S. Effect of Interfacial Interaction on Morphology and Properties of Polyethylene/Boron Nitride Thermally Conductive Composites. *Polym.-Plast. Technol. Eng.* **2015**, *54*, 1097−1105.
(69) Muratov, D. S.; Stepashkin, A. A.; Anshin, S. M.; Kuznetsov, D. V. Controlling Thermal Conductivity of High Density Polyethylene Filled with Modified Hexagonal Boron Nitride (hBN). *J. Alloys Compd.* **2018**, *735*, 1200−1205.
(70) Shin, J. W.; Lee, J.-W.; Yu, S.; Baek, B. K.; Hong, J. P.; Seo, Y.; Kim, W. N.; Hong, S. M.; Koo, C. M. Polyethylene/Boron-Containing Composites for Radiation Shielding. *Thermochim. Acta* **2014**, *585*, 5−9.
(71) Zhao, T.; Zhang, X. Enhanced Thermal Conductivity of PE/BN Composites through Controlling Crystallization Behavior of PE Matrix. *Polym. Compos.* **2017**, *38*, 2806−2813.
(72) Zhou, W.; Qi, S.; An, Q.; Zhao, H.; Liu, N. Thermal Conductivity of Boron Nitride Reinforced Polyethylene Composites. *Mater. Res. Bull.* **2007**, *42*, 1863−1873.
(73) Borjas-Ramos, J. J.; Ramos-de-Valle, L. F.; Neira-Velázquez, M. G.; Hernández-Hernández, E.; Saucedo-Salazar, E. M.; Soria-Argüello, G. Thermal Conductivity of Nanocomposites Based in High Density Polyethylene and Surface Modified Hexagonal Boron Nitride via Cold Ethylene Plasma. *Plasma Chem. Plasma Process.* **2018**, *38*, 429−441.
(74) Che, J.; Jing, M.; Liu, D.; Wang, K.; Fu, Q. Largely Enhanced Thermal Conductivity of HDPE/Boron Nitride/Carbon Nanotubes Ternary Composites via Filler Network-Network Synergy and Orientation. *Composites, Part A* **2018**, *112*, 32−39.
(75) Zhao, T.; Zhang, X. Synergistic Effect of Thermally Conductive Networks in Crystalline Polymer Composites. *Polym. Compos.* **2018**, *39*, 1041−1050.
(76) Wang, Z.; Li, Q.; Chen, Z.; Li, H.; Zheng, S.; Tang, X. Functionalization of Boron Nitride Nanosheets by Diazonium Salt for Preparation of Nanocomposites with High-Density Polyethylene. *Polym. Compos.* **2018**, DOI: 10.1002/pc.25093.

DOI: 10.1021/acsanm.8b01992
ACS Appl. Nano Mater. 2019, 2, 440−451